ISSN 1063-7710, Acoustical Physics, 2014, Vol. 60, No. 4, pp. 387–397. © Pleiades Publishing, Ltd., 2014.
Original Russian Text © E.G. Lobanova, S.V. Lobanov, V.A. Khokhlova, 2014, published in Akusticheskii Zhurnal, 2014, Vol. 60, No. 4, pp. 356–367.

NONLINEAR ACOUSTICS

Counterpropagation of Waves with Shock Fronts in a Nonlinear Tissue-Like Medium

E. G. Lobanova[a], S. V. Lobanov[b], and V. A. Khokhlova[a, c]

[a] *Physics Faculty, Moscow State University, Moscow, 119991 Russia*
e-mail: moreva@physics.msu.ru, vera@acs366.phys.msu.ru
[b] *Skolkovo Institute of Science and Technology, ul. Novaya 100, Skolkovo, Moscow oblast, 143025 Russia*
[c] *Center for Industrial and Medical Ultrasound, Applied Physics Laboratory, University of Washington, Seattle, Washington, 98105 USA*

Received February 5, 2014

Abstract—A numerical model for describing the counterpropagation of one-dimensional waves in a nonlinear medium with an arbitrary power law absorption and corresponding dispersion is developed. The model is based on general one-dimensional Navier–Stokes equations with absorption in the form of a time-domain convolution operator in the equation of state. The developed algorithm makes it possible to describe wave interactions in the presence of shock fronts in media like biological tissue. Numerical modeling is conducted by the finite difference method on a staggered grid; absorption and sound speed dispersion are taken into account using the causal memory function. The developed model is used for numerical calculations, which demonstrate the absorption and dispersion effects on nonlinear propagation of differently shaped pulses, as well as their reflection from impedance acoustic boundaries.

Keywords: relaxation, dispersion, nonlinearity, full wave equation
DOI: 10.1134/S1063771014040071

1. INTRODUCTION

The fundamental problem of nonlinear counterpropagation of acoustic waves in inhomogeneous lossy media is one of the most promising directions in modern acoustics. In many respects, this is related to the development of novel applications of high intensity ultrasound in medicine [1–3]. For instance, ultrasonic echography using higher harmonics [4, 5], focused ultrasound shock pulses to destroy kidney stones (extracorporeal lithotripsy) [6, 7], and noninvasive ultrasound surgery [8, 9] are examples of the emerging medical technologies. The main results in this field have been obtained for unidirectional propagation of plane waves and acoustic beams in water and biological tissues described by model nonlinear equations of the evolution type [2–6, 8–10]. However, to solve practically important problems of visualizing therapeutic effects on tissue with ultrasound and evaluation of its safety in irradiation through various types of tissue layers, it is often necessary to take into account the effects of reflections and scattering. In this case, the question arises of constructing and solving a full nonlinear wave equation where results to date are scarce [7, 11, 12]. In constructing a full wave model, it is important that it includes frequency-dependent absorption and dispersion that satisfy the experimental data and correspond to the causality principle.

As is known, the wave equation for a classical thermoviscous fluid contains a derivative operator that governs absorption, proportional to the frequency squared. The absorption mechanisms in soft biological tissues are significantly more complex and are related to various types of vibrational, structural, and chemical relaxation, which leads to the experimentally observed frequency power law absorption in the form

$$\alpha(\omega) = \alpha_0 \left|\frac{\omega}{\omega_0}\right|^{\eta}, \quad \eta = y + 1, \tag{1}$$

where α_0 is the absorption coefficient at frequency ω_0, ω is the angular frequency, and the power law exponent η typically varies from 1 to 1.5 [1].

To take this difference into account, the lossy derivative operator for a thermoviscous fluid is replaced by a general absorption operator. Rudenko, Soluyan, and Khokhlov proposed writing the lossy operator in the Khokhlov–Zabolotskaya–Kuznetsov (KZK) equation in general integral form as a convolution of the solution with a kernel governing an arbitrary frequency law absorption in the medium [13]. Different specific forms of the integral operators to account for frequency power law absorption were obtained later in the papers by O'Donnell [14], Collins [15], and Szabo [16]. An alternative approach, which approximates the power law absorption (1) as the sum of the relaxation processes, has also been proposed.

Such an approach corresponds to the relationship between absorption in tissue and various relaxation processes. Models of continuous distribution of the relaxation parameters [17] and a discrete set of several relaxation processes have been proposed [18]. It was shown that two relaxation processes quite accurately approximate the power law absorption in the range of 1–12 MHz [19].

When implemented numerically, the integral form of the absorption operator substantially slows the calculations. As an alternative, Chen and Nolm obtained a lossy operator based on the fractional Laplacian in nonlinear acoustics equations [20]. This operator was later generalized by taking into account a dispersion of the sound speed as required by the Kramers–Kronig relations [21]. In comparison to the time domain convolution operator, calculation of the fractional Laplacian depends only on the pressure field values at current time instants. This makes the operator efficient to compute, particularly using the pseudospectral and *K*-space methods [22].

Simulation of acoustic wave propagation in media with frequency power law absorption $|\omega|^{\eta}$ thus reduces to introducing into the wave equation the fractional Laplacian $(-\nabla^2)^{\eta/2}$ in spatial coordinates or the integral time-domain operator of absorption. Construction of the integral operator itself, which corresponds to the power law absorption and the causality principle, is still ambiguous and interesting scientific problem.

This paper proposes a novel approach that makes it possible, proceeding from the known frequency dependence of absorption, to calculate the memory function in the integral operator of losses. Using this method, the frequency dependence of absorption should not necessarily be written as an analytic function, but, e.g., it can be obtained in experiment or has a complex form when it is impossible to calculate the sound speed dispersion using local dispersion relations. A system of equations for one-dimensional counterpropagating waves that accounts for the effects of nonlinearity, absorption, and dispersion is obtained. A finite difference algorithm for modeling the system is developed. The accuracy of the algorithm is examined by solving a number of benchmark acoustic problems that have analytical solutions. New results in the problem on nonlinear pulse propagation in a medium like biological tissue and its reflection from a soft boundary are obtained.

2. THEORETICAL METHOD

2.1. Method of Constructing the Causal Integral Operator for the Power Law Absorption

Let us describe one-dimensional wave motion in a nonlinear medium with memory by a system of equations like hydrodynamics for acoustic waves:

$$\frac{\partial u}{\partial t} = -\frac{1}{\rho_0 + \rho'}\frac{\partial p'}{\partial x} - \frac{1}{2}\frac{\partial u^2}{\partial x}, \tag{2}$$

$$\frac{\partial \rho'}{\partial t} = -\frac{\partial}{\partial x}\left[(\rho_0 + \rho')u\right], \tag{3}$$

$$p' = c_0^2 \int_0^{+\infty} S(t')\rho'(t-t')dt' + \frac{1}{2}\frac{\varepsilon - 1}{\rho_0}c_0^2\rho'^2, \tag{4}$$

where ρ' and p' are the density and pressure deviations from their equilibrium values: $\rho = \rho_0(x) + \rho'$, $p = p_0 + p'$; u is the particle velocity in the medium; $\rho_0(x)$ is the ambient density; $c_0(x)$ is the sound speed; ε is the parameter of acoustic nonlinearity. The equation of state (4) is written as the convolution in the time domain. From here on, kernel $S(\tau)$ in integral law absorption (4) will be called the memory function of the propagation medium. Linearization of the system of equations (2)–(4) for a homogeneous medium yields a wave equation with respect to the perturbation of the ambient density ρ':

$$\frac{1}{c_0^2}\frac{\partial^2 \rho'}{\partial t^2} - \frac{\partial^2}{\partial x^2}\left[\int_0^{+\infty} S(t')\rho'(t-t')dt'\right] = 0. \tag{5}$$

The proposed method of obtaining the dispersion equation for (5) and reconstructing on its basis the form of kernel $S(t)$ in integral relation (4) consists of the following. We seek the solution (5) in the form of a traveling wave:

$$\rho' = \rho'_0 \exp\left(-i(\omega t + kx)\right), \tag{6}$$

where the complex wavenumber k has the form

$$k(\omega) = k'(\omega) + ik''(\omega) = \frac{\omega}{c(\omega)} + i\alpha(\omega). \tag{7}$$

Here $k''(\omega) = \alpha(\omega)$ describes the frequency dependence of the absorption law and $c(\omega)$ is the dispersion law. Substitution of the expression (6) for the perturbed density ρ' in the wave equation (5) yields the dispersion relation

$$k(\omega) = \frac{\omega}{c_0}S^{-0.5}(\omega), \tag{8}$$

where $S(\omega)$ is determined, taking into account the causality principle, as

$$S(\omega) = \int_0^{+\infty} S(t')e^{i\omega t'}dt'. \tag{9}$$

Equalizing the right-hand sides of the relations (7) and (8) for wavenumber k, we obtain the expression for memory function $S(\omega)$ in the frequency representation:

$$S(\omega) = \left(\frac{c_0}{c(\omega)} + i\frac{c_0\alpha(\omega)}{\omega}\right)^{-2}. \tag{10}$$

Expression (10) can easily be rewritten in the form of relations expressing absorption $\alpha(\omega)$ and sound speed dispersion $c(\omega)$ using the memory function $S(\omega)$:

$$\alpha(\omega) = \frac{\omega}{c_0}\mathrm{Im}\left[S^{-0.5}(\omega)\right],$$
$$c(\omega) = c_0\left(\mathrm{Re}\left[S^{-0.5}(\omega)\right]\right)^{-1}. \quad (11)$$

In the expression (11), the dependence $c(\omega)$ is unknown. However, it is known that variations in sound speed with frequency in biological tissues are small [1]. Thus, we will seek $S(\omega)$ by the method of successive approximations, limiting ourselves to the first approximation. For this, absorption $\alpha(\omega)$ and sound speed dispersion $c(\omega)$ are represented as

$$\alpha(\omega) = \alpha^{(0)}(\omega) + \alpha^{(1)}(\omega) = \alpha_0\left|\omega/\omega_0\right|^{y+1} + \Delta\alpha(\omega),$$
$$\Delta\alpha(\omega) \ll \alpha_0, \quad (12)$$
$$c(\omega) = c^{(0)} + c^{(1)}(\omega) = c_0 + \Delta c(\omega), \quad \Delta c(\omega) \ll c_0.$$

If we now substitute the relations (12) for absorption $\alpha(\omega)$ and sound speed dispersion $c(\omega)$ in the expression for $S(\omega)$ (10), then, after a number of transformations that approximate the attenuation length as being much larger than the wavelength of the acoustic field, $\alpha(\omega) \ll \omega/c(\omega)$, we come to the expression

$$S(\omega) = 1 - 2i\frac{c_0\alpha(\omega)}{\omega} + 2\frac{\Delta c(\omega)}{c_0} - 2i\frac{\Delta\alpha(\omega)c_0}{\omega}. \quad (13)$$

In expression (13), the first two terms are the zero approximation $S^{(0)}(\omega)$, expressing the absence of sound speed dispersion $\mathrm{Re}\{S^{(0)}(\omega)\}$, and the given frequency dependence $\mathrm{Im}\{S^{(0)}(\omega)\}$ of absorption per wavelength. The last two terms describe the relative correction to the equilibrium sound speed $\Delta c(\omega)/c_0$, expressing the dispersion law $\mathrm{Re}\{S^{(1)}(\omega)\}$, and the artificial addition $\Delta\alpha(\omega)c_0/\omega$ to the law of absorption per wavelength $\mathrm{Im}\{S^{(1)}(\omega)\}$. Thus, expression (13) is the first approximation for $S^{(1)}(\omega)$.

We now pass directly to constructing the causal kernel $S(t')$ in the integral law absorption, using the method of successive approximations, which consists of two steps. At the first step, if we neglect the sound speed dispersion and use the expression (1) for absorption in relation (10), we then obtain

$$S(\omega) = \left(1 + ic_0\alpha_0\left|\omega\right|^y \mathrm{sgn}(\omega)\right)^{-2}. \quad (14)$$

Expression (14) is the zero approximation of $S^{(0)}(\omega)$. However, such an expression does not satisfy the causality principle. This is easy to demonstrate by performing the inverse Fourier transform on formula (14), i.e., transferring from the frequency representation of memory function $S(\omega)$ to the time representation $S(t')$:

$$S(t') = \frac{1}{2\pi}\int_{-\infty}^{+\infty} S(\omega)e^{-i\omega t'}d\omega$$
$$= \frac{1}{2\pi}\int_{-\infty}^{+\infty}\left(1 + ic_0\alpha_0\left|\omega\right|^y \mathrm{sgn}(\omega)\right)^{-2} e^{-i\omega t'}d\omega. \quad (15)$$

One can see from the obtained expression that memory function $S(t') \neq 0$ for $t' < 0$. Integral (15) can be reconstructed analytically in rare cases; therefore, we will calculate function $S(t')$ numerically at the nodes of the numerical temporal grid $\tau_n = \tau n$:

$$S(\tau_n) = \frac{1}{2\pi}\int_{-\infty}^{+\infty} S(\omega)\,\mathrm{sinc}(0.5\omega\tau)\exp\left(-i\omega\tau n\right)d\omega, \quad (16)$$

where $n = \overline{0,\ N-1}$, N is the number of grid points used in calculating the memory function $S(\tau_n)$, and τ is the time step of the grid. Since the memory function is a real quantity, its spectrum $S(-\omega) = S^*(\omega)$. Using this property, we obtain

$$S(\tau n) = \frac{1}{2\pi}\int_0^{+\infty} 2\,\mathrm{Re}(S(\omega)e^{-i\omega\tau n})\,\mathrm{sinc}(0.5\omega\tau)d\omega$$
$$= \frac{1}{\pi}\int_0^{+\infty}\left[\frac{1 - \alpha_0^2c_0^2\left|\omega\right|^{2y}}{\left(1 + \alpha_0^2c_0^2\left|\omega\right|^{2y}\right)^2}\cos(\omega\tau n)\right. \quad (17)$$
$$\left. - 2\frac{\alpha_0c_0\left|\omega\right|^y\mathrm{sgn}(\omega)}{\left(1 + \alpha_0^2c_0^2\left|\omega\right|^{2y}\right)^2}\sin(\omega\tau n)\right]\mathrm{sinc}(0.5\omega\tau)d\omega.$$

At the second step, to satisfy the causality principle, we set the memory function $\tau < 0$ for $S(\tau_n) = 0$ in the expression (17). If we now perform direct Fourier transform of the expression (17) taking into account that $S(\tau n) = 0$ for $\tau < 0$, then the causal memory function $S^{(1)}(\omega)$ will be reconstructed in the first approximation. Figure 1 shows the behavior of the non-casual $S^{(0)}$ (black dashed curve) and causal $S^{(1)}$ (solid gray curve) memory functions in the frequency and time representations. Figure 1b shows memory function $S(f)$ as a function of frequency $f = \omega/2\pi$. The absorption law was chosen in the form $\alpha = \alpha_0|f/f_0|^{1.05}$, the absorption coefficient α_0 at a frequency of 1 MHz was 0.45 dB/cm, and the sound speed was $c_0 = 1578$ m/s, which corresponds to the experimental data for the liver [1]. One can see from Fig. 1b that the difference between the curves $\mathrm{Re}\{S^{(0)}(f)\}$ (no dispersion) and $\mathrm{Re}\{S^{(1)}(f)\}$ (dispersion is taken into account in (13) in the form of the relative correction to the equilibrium sound speed) is less than 1.5%. The curve $\mathrm{Im}\{S^{(0)}(f)\}$ describing the exact frequency law absorption per wavelength (13), and the curve $\mathrm{Im}\{S^{(1)}(f)\}$, responsible for the appearance of the artificial addition to the absorption law, are virtually indistinguishable in the frequency range from 0 to 35 MHz. As a result, proceeding from Fig. 1b, we can obtain (1) the relative correction to the equilibrium sound speed $\Delta c(f)/c_0$ as the half-difference of the real parts of the memory function spectra in the first and zero approximations $0.5\left(\mathrm{Re}\left\{S^{(1)}(f)\right\} - \mathrm{Re}\left\{S^{(0)}(f)\right\}\right)$ and (2) the artificial addition $\Delta\alpha(f)c_0/f$ to the absorption law per wavelength according to the expression

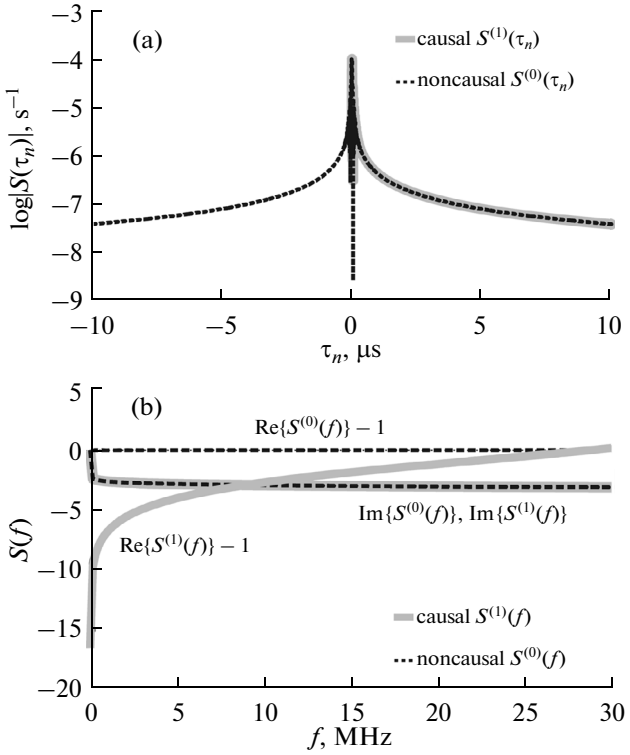

Fig. 1. Time dependences of the absolute values of noncausal $S^{(0)}(\tau n)$ (dashed black curve) and causal $S^{(1)}(\tau n)$ (solid gray line) memory function (a). Frequency dependences of the real and imaginary parts of noncausal $S^{(0)}(f)$ (dashed black curve) and causal $S^{(1)}(f)$ (solid gray curve) memory function (b).

$0.5\left(\mathrm{Im}\left\{S^{(1)}(f)\right\} - \mathrm{Im}\left\{S^{(0)}(f)\right\}\right)$, the dependence of which is shown in Fig. 2. One can see from Fig. 2 that the relative correction to the equilibrium sound speed (gray curve) expressing the dispersion law is less than 1%. The artificial addition to the absorption law per wavelength (black curve) is less than 2×10^{-5} in the frequency range from 0 to 30 MHz; i.e., the error introduced into the exact absorption law is small. Thus, our method of constructing a causal kernel $S(t')$ in the integral law absorption gives, in the first order of successive approximations, a good accuracy for media like biological tissues; it is also applicable for describing the effects of absorption and dispersion in other weakly dispersive media.

Thus, in the zero approximation, the absorption law $\alpha(\omega)$ is exact, there is no dispersion, but memory function $S^{(0)}$ does not satisfy the causality principle (14), (15). In the first approximation, to satisfy the causality principle, the memory function $S^{(0)}(t')$ is artificially zeroized for $t' < 0$ and its causal form $S^{(1)}$ is automatically obtained. As a result, the correction $\Delta c(\omega)$ to the equilibrium sound speed appears, as well as the artificial addition $\Delta\alpha(\omega)$ to the absorption law, which is less than 1% in the frequency range from 0 to 30 MHz. Equations (2)–(4) with

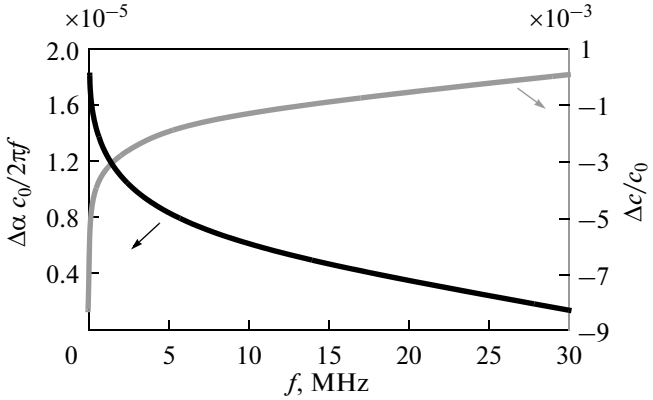

Fig. 2. Relative correction to the ambient sound speed $\Delta c(f)/c_0$ (gray curve) and artificial addition $\Delta\alpha(f)c_0/f$ (black curve) to the absorption law per wavelength as a function of frequency in the range from 0 to 30 MHz.

causal kernel (17) are further used to construct the numerical model.

2.2. Numerical Model

In the work, the system of equations (2)–(4) was numerically solved within the spatial segment $(-x_0; L + x_0)$ with zero initial conditions (Fig. 3):

$$p'(x,\ t = 0) = 0,\quad u(x,\ t = 0) = 0,\quad \rho'(x,\ t = 0) = 0. \quad (18)$$

As boundary conditions, depending on the problem, a rigid (19a) or soft boundary (19b) was used:

$$u(x = x_\mathrm{b}, t) = 0,\quad \frac{\partial p}{\partial x}(x = x_\mathrm{b}, t) = 0, \quad (19a)$$

$$\frac{\partial u}{\partial x}(x = x_\mathrm{b}, t) = 0,\quad p(x = x_\mathrm{b}, t) = 0, \quad (19b)$$

where $x_\mathrm{b} = -x_0$ or $L + x_0$ is the boundary of the considered spatial domain.

To simulate a wave moving freely away to infinity, so-called PMLs (perfectly matched layers) [23] were placed near the border of the considered domain $(-x_0; L + x_0)$, which ensured non-reflective propagation of waves incident on them and corresponded to the segments $(-x_0; 0)$ and $(L; L + x_0)$. The length x_0 of a PML was a fraction of a percent of the length of the considered spatial domain $(-x_0; L + x_0)$. The numerical algorithm was implemented in such a way that at a certain point x_1, the internal source of ultrasound waves was introduced in the form of a pulse of a certain shape $u(x_1, t)$.

2.3. Numerical Algorithm

To use the finite difference method when modeling the system of equations (2)–(4) with kernel (17) in the equation of state, function $u(x, t)$ was defined at the

grid nodes of the spatial coordinate x and time coordinate t as $u_{q,s}$, and $\rho'(x, t)$ in the nodes of a grid shifted by half a step, as $\rho'_{q-1/2,s-1/2}$ and $\rho'_{q-1/2,s-1/2}$:

$$u_{q,s} = u(x_q, t_s), \quad p'_{q-1/2,s-1/2} = p'(x_{q-1/2}, t_{s-1/2}), \quad \rho'_{q-1/2,s-1/2} = \rho'(x_{q-1/2}, t_{s-1/2}). \tag{20}$$

After the derivatives in the system of equations (2)–(4) were replaced with finite difference terms, the system takes the form

$$u_{q+1,s+1} = u_{q+1,s} - \tau \frac{2}{\rho_{q+1/2,s+1/2} + \rho_{q+3/2,s+1/2}} \times \frac{p'_{q+3/2,s+1/2} - p'_{q+1/2,s+1/2}}{h} - \tau \frac{u^2_{q+2,s} - u^2_{q,s}}{4h}, \tag{21}$$

$$\rho'_{q+1/2,s+1/2} = \rho'_{q+1/2,s-1/2} - \tau \frac{(\rho_{q-1/2,s-1/2} + \rho_{q+1/2,s-1/2})u_{q,s} - (\rho_{q+1/2,s-1/2} + \rho_{q+3/2,s-1/2})u_{q+1,s}}{2h}, \tag{22}$$

$$p'_{q+1/2,s+1/2} = c_0^2 \sum_{n=0}^{N-1} \rho'(x_{q+1/2}, t_{s+1/2} - \tau n) S(\tau n) + \frac{1}{2} \frac{\varepsilon - 1}{\rho_0^{q+1/2}} c_0^2 \rho'^2_{q+1/2,\,s-1/2}, \tag{23}$$

where τ is the time step and h is the step along the spatial coordinate. In expressions (21)–(22), for each grid point $x_{q-1/2,s-1/2}$, $\rho_{q-1/2,\,s-1/2} = \rho_0(x_{q-1/2}) + \rho'_{q-1/2,\,s-1/2}$.

The algorithm was implemented such that at each time step, the finite difference equation (22) for the perturbed density $\rho'_{q+1/2,s+1/2}$ was solved first (Fig. 4a). Then, over its entire time history in the form of the preceding N steps, the acoustic pressure $p'_{q+1/2,s+1/2}$ from expression (23) was calculated. At the final stage, from the known values $\rho'_{q+1/2,s+1/2}$ and $p'_{q+1/2,s+1/2}$, the value of the particle velocity $u_{q+1,\,s+1}$ from the equation (21) was obtained (Fig. 4b).

3. RESULTS AND DISCUSSION

Below we present the results of using the proposed method to construct the causal memory function and to simulate the system of equations (21)–(23), illustrating the effects of wave propagation in two directions, nonlinearity, absorption, dispersion, and reflection from the impedance boundary. Two well-known model problems are examined here such as propagation of a single pulse in a thermoviscous medium, which demonstrates the accuracy of the representation of the absorption operator on the grid and the absence of numerical viscosity and dispersion; and nonlinear propagation of a plane wave, which illustrates the accuracy in describing the nonlinear finite difference operator. We then consider the problem of how different physical effects influence on the waveform structure: propagation and reflection from a soft acoustic boundary of a unidirectional pulse in a nonlinear medium with memory and in a medium without memory. We further study the problem of reflection of a shock pulse from a soft acoustic boundary. This problem imitates the reflection of ultrasound waves with shocks from a vapor bubble when boiling in tissue is initiated at the focus of high intensity focused ultrasound (HIFU) transducers. This situation occurs in problems on applying HIFU in noninvasive surgery and is of interest for studying the corresponding mechanisms of biological tissue damage. All calculations were performed mainly with the time step of $\tau = 300$ ps and the spatial step of $h = 0.5$ μm.

Figure 5 shows the dependences of the absorption coefficient $\alpha(f)$ normalized to its value α_0 at 1 MHz, and variations in the sound speed $\Delta c(\omega)/c_0$ for media with a different power law exponent η, calculated by the proposed method (solid curve) and using local dispersion relations developed by Szabo (circles) [1, 16]. The curves in the figure have been constructed for blood ($\eta = 1.42$, $\alpha_0 = 0.22$ dB/cm, $c_0 = 1570$ m/s), liver ($\eta = 1.2$, $\alpha_0 = 0.71$ dB/cm, $c_0 = 1600$ m/s) [1], water ($\eta = 2$, $\alpha_0 = 0.0025$ dB/cm, $c_0 = 1500$), and butanediol ($\eta = 1$, $\alpha_0 = 0.33$ dB/cm, $c_0 = 1546$ m/s). Figure 5a shows the dependences for absorption coefficient $\alpha(f)$ neglecting (circles) and taking into account (solid line) the correction to the absorption law $\Delta\alpha(f)$ that corresponds to the causality principle.

One can see from Fig. 5b that the sound speed dispersion is indeed small, less than 1% in soft tissues within the range from 1 to 10 MHz. In the case of clas-

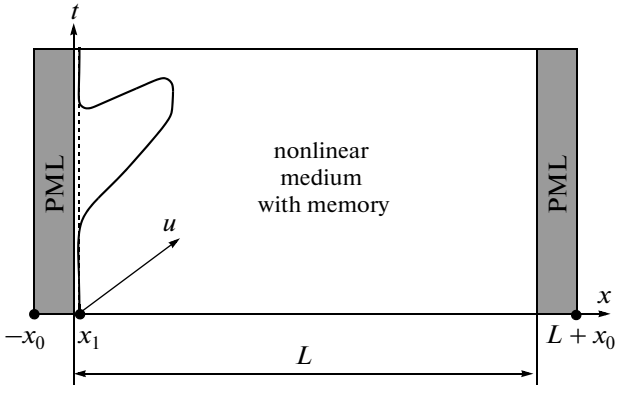

Fig. 3. Schematic diagram of the coordinate system used in simulations with the initial and boundary conditions. The vertical dashed line shows the position of the internal source, and the adjacent solid curve shows a single pressure pulse as an example of the time-dependent boundary condition.

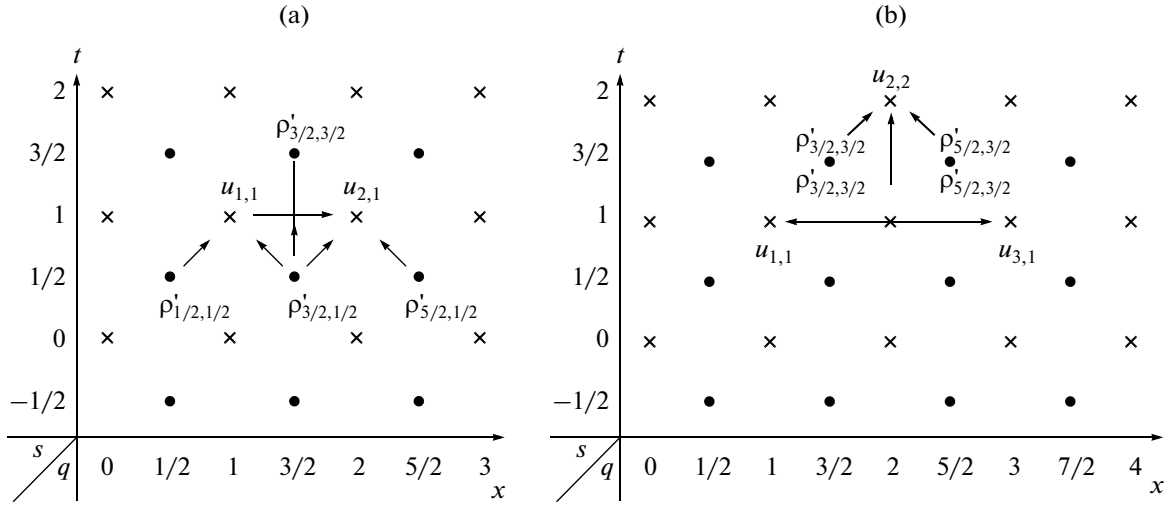

Fig. 4. Diagram of constructing the solution on a staggered grid for the perturbed density (a) and particle velocity (b) in counter-propagating acoustic wave.

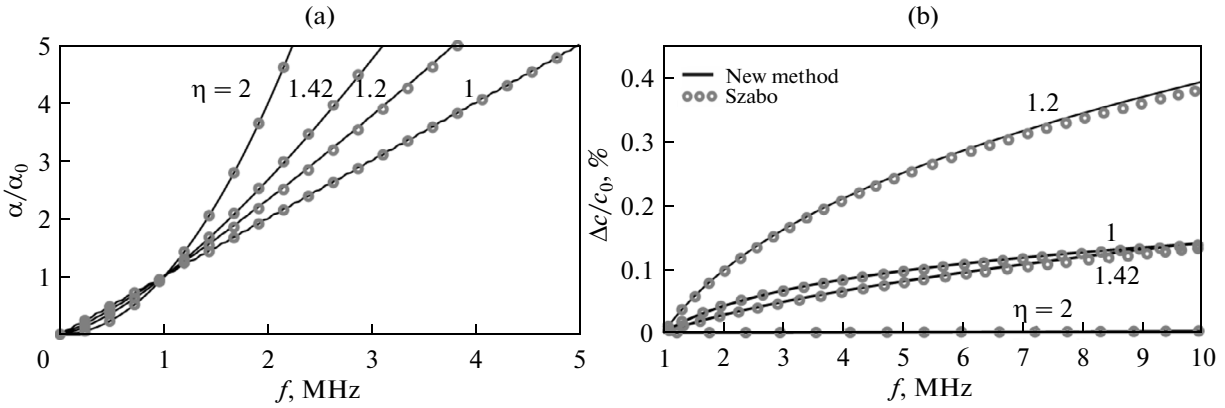

Fig. 5. Dependences of the absorption coefficient $\alpha(f)$ normalized to its value α_0 at 1 MHz and of the relative change in sound speed $\Delta c(\omega)/c_0$ for media with different power law exponents η (numerals on curves), calculated by the proposed method (solid curve) and using local dispersion relations developed by Szabo (circles).

sical quadratic absorption, the dispersion is absent. The difference in determining the dispersion law using the two approaches is fractions of a percent. In contrast to Szabo's model of local dispersion relations, where the dispersion curves can be calculated for a particular type of absorption law, our method makes it possible to calculate the sound speed dispersion for any absorption law, which can have a complex form or lack an analytic expression, e.g., being obtained in experiment.

Figure 6 shows the simulation results describing the broadening of a Gaussian pulse with initial amplitude of $p_0 = 5$ MPa in a linear medium with a quadratic frequency law absorption $\eta = 2$. Clearly, the numerical calculations with sufficiently small grid steps (dashed black curve) agree well with the known analytic solution to the linearized Burgers equation in the form of convolution of the Green's function of a point source with an initial perturbation of the Gaussian profile of $p'(x = 0, t) = p'_0(t)$ (solid gray curve) [1]:

$$p'(x, t) = p_0\left(1 + \frac{4\delta x}{T_0^2}\right)^{-0.5} \exp\left[-\frac{(t - x/c_0)^2}{T_0^2 + 4\delta x}\right], \quad (24)$$

where $\delta = \alpha_0/(8.686\omega_0^2) = 0.13 \times 10^{-12}$ s^2 m^{-1} is the sound absorption coefficient that corresponds to the quadratic frequency law $\alpha = \alpha_0(\omega/\omega_0^2)$. Here, the coefficient α_0 at a frequency of $f_0 = \omega_0/2\pi = 1$ MHz was 0.45 dB/cm, like in biological tissue; the pulse duration was $2T_0 = 1$ μs; the sound speed was $c_0 = 1500$ m/s; the attenuation length at which the pulse amplitude decreased by e times was about 3 m.

In this problem, to calculate a smooth wave profile, the spatial step h was chosen as 5 μm and the time step τ was chosen as 3 ns, in accordance with the Cou-

rant criterion. For a width of the initial Gaussian pulse (dashed black curve) of 1.5 mm, this corresponded to approximately 300 points per initial pulse width. Clearly, such discretization was sufficient so that the effects of numerical viscosity and dispersion were not significant during the propagation up to the distance of around 2000 initial pulse widths (3 m), i.e., one attenuation length. The figure also shows the solution for large grid steps $h = 250$ μm and $h = 30$ ns (dashed gray line), illustrating the effect of numerical viscosity and dispersion. When choosing the step of $h = 5$ μm, the deviation from the exact solution at a distance of around 2000 initial pulse widths (3 m) was slightly less than half a percent, and for the 50 times larger step ($h = 250$ μm), it was around 27%.

Now consider the problem of nonlinear propagation of nonlinear Riemann waves, which has an exact analytic solution. This solution follows from the system of the Euler equations in the case of the adiabatic equation of state and in the small Mach number approximation:

$$p' = \Phi\left(t \mp x c_0^{-1} + \varepsilon \rho_0^{-1} c_0^{-3} p' x\right), \qquad (25)$$

where the function $\Phi(t) = p'(x = 0, t)$ gives the temporal wave profile at the entrance to a nonlinear medium. Expression (25) describes noninteracting nonlinear waves traveling both in the positive and negative directions of axis x; the upper symbols correspond to the wave traveling to the right.

Figure 7 shows the results of simulating the unidirectional propagation of a simple wave traveling in the positive direction (right). The initial pulse had a Gaussian shape $p'(x = 0, t) = p_0 \exp\left(-t^2/T_0^2\right)$ with the amplitude of $p_0 = 5$ MPa and the duration of $2T_0 = 1$ μs; the parameters of the nonlinear medium c_0, ρ_0, ε were close to those of biological tissue ($c_0 = 1578$ m/s, $\rho_0 = 1060$ kg/m^3, $\varepsilon = 4.38$) [1]. The solid curves in the figure have been calculated numerically using the developed algorithm and are compared to the dashed curves obtained from the exact solution to the simple wave equation

$$p' = p_0 \exp\left\{-\left(\frac{\tau + \varepsilon \rho_0^{-1} c_0^{-3} p' x}{T_0}\right)^2\right\}. \qquad (26)$$

In the expression (26), the variable $\tau = t - x/c_0$ is time in the traveling coordinate system. If we pass from an implicit $p'(x, \tau)$ to an explicit solution $\tau(x, p')$ in the formula (26), we obtain

$$\tau = T_0 \sqrt{\ln\left(p_0/p'\right)} - \left(\varepsilon/\rho_0 c_0^3\right) p' x. \qquad (27)$$

To construct the solution, we simply need to add the initial wave profile $\tau = \Phi^{-1}(p') = T_0 \sqrt{\ln\left(p_0/p'\right)}$ to the linear function $\Delta\tau = -\left(\varepsilon/\rho_0 c_0^3\right) p' x$.

As well known from theory and confirmed by numerical calculation, during propagation, the parts of acoustic waveform with higher positive pressure propagate faster and as a result "overrun" the waveform parts with lower pressure, the speed of which is lower. As a result, waveform parts with increasing pressure become steeper, and waveform parts with decreasing pressure, vice versa, become smoother. As one can see from the Fig. 7, at a distance of $x_p = \sqrt{\frac{e}{2}} \frac{\rho_0 c_0^3 T_0}{\varepsilon p_0}$, which for the given parameters of the problem corresponds to 11.1 cm, the tangent to the profile at the point $\tau_p = T_0/\sqrt{2}$ becomes vertical, and for further increase in distance, an ambiguity arises: it "tips over."

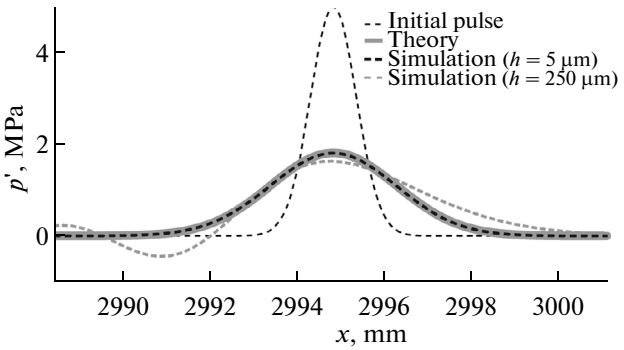

Fig. 6. Comparison of exact (gray solid curve) and numerical (black dashed curve) solutions for the initial Gaussian pulse (thin black dashed line) with the amplitude of $p_0 = 5$ MPa and duration of 1 μs after propagation at a distance of 3 m in the medium with an absorption coefficient of $\alpha_0 = 0.45$ dB/cm at a frequency of 1 MHz for different grid steps of $h = 5$ μm and $h = 250$ μm.

Figure 7 depicts a similar profile at the distance of $x = 4x_p$ that was calculated analytically taking into account the "rule of equal areas," i.e., cutting off the areas of ambiguity, as a result of which the profile converts to a triangular shape. As one can see, the profiles calculated numerically (dashed black curves) are virtually superposed on the profiles having an analytic solution in the form of Riemann waves (solid gray curves) with one characteristic difference: the shock fronts in the exact Riemann solution with allowance for the rule of equal areas is vertical; for the numerical profile, the shock front has a finite width. This discrepancy is related to the impossibility of describing wave solutions with mathematical discontinuities using the finite difference method: the given time instant and point in space should singularly determine the parameters p', u, and ρ'. Therefore, in numerical calculations, in order to construct a solution with a shock front, a nonlinear viscous medium was considered, having a small viscosity quadratic with frequency that smoothens the wave front. For the given problem, the following parameters of such a medium were chosen: the absorption coefficient α_0 at a frequency of 1 MHz was 10^{-2} dB/cm, the sound speed was $c_0 = 1578$ m/s, the density was $\rho_0 = 1060$ kg/m^3, and the parameter of acoustic nonlinearity was $\varepsilon = 4.38$,

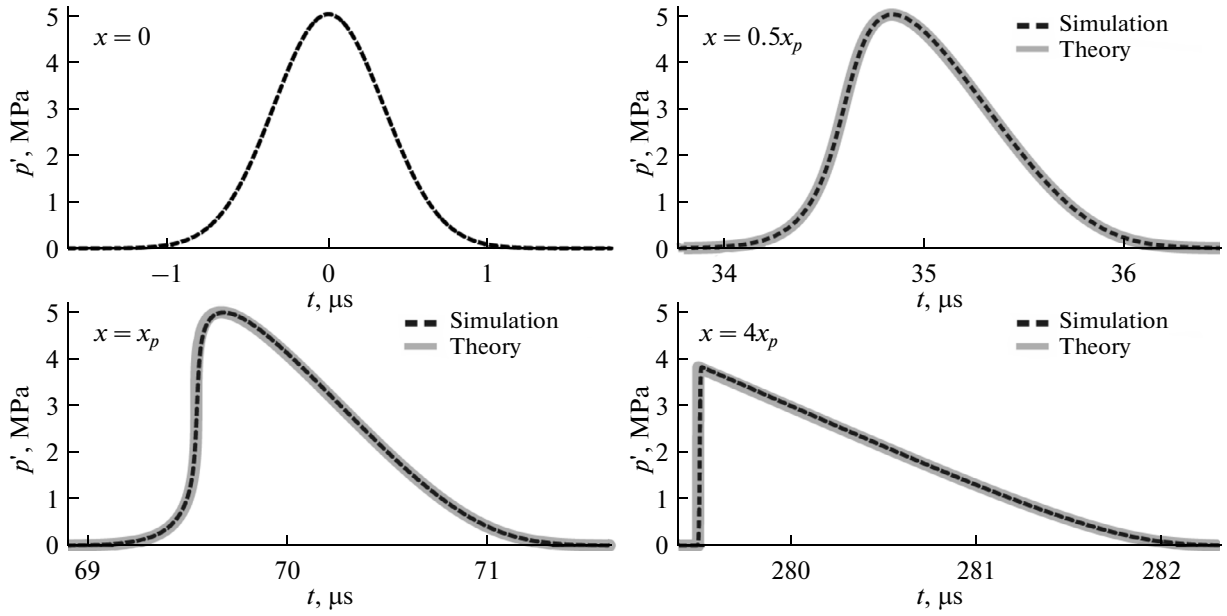

Fig. 7. Distortion of the initial Gaussian pulse with an amplitude of $p_0 = 5$ MPa and duration of 1 μs while propagating in a nonlinear medium with a parameter of acoustic nonlinearity of $\varepsilon = 4.38$: numerical calculation (black dashed curves) and analytic solution (gray solid curves) of the simple wave equation.

which for a time step of $\tau = 0.3$ ps corresponded to 80 points per shock front. Clearly, such discretization sufficed to describe wave propagation up to the distance of four shock formation lengths, or 277 initial pulse lengths, without manifestation of numerical viscosity and distortion of the shocks in the pulse.

Figure 8 shows the results of simulating nonlinear counterpropagation of two pulses at different time instants t. The distance between the initial pulses was $8x_p$ (88.8 cm); their amplitudes, durations, shapes, and parameters of the medium were chosen as in the case of the unidirectional propagation (Fig. 7). The dashed black curves in the figure were calculated numerically using our algorithm and are compared to the solid gray curves, which are the superposition of two exact solutions to the simple wave equation, which correspond to pulse propagation in opposite directions (25). Collision of pulses begins at the time instant $t = 279.4$ μs. At the time instant $t = 279.51$ μs, during the collision of pulses, the numerically calculated profiles are indistinguishable from the analytic solutions in the form of a superposition of noninteracting Riemann waves. After interaction, at the time instant $t = 286.58$ μs, the pulse divides into two pulses, which coincide in shape with those observed before the collision. Thus, despite the nonlinearity of the process, for the pulse amplitude of 5 MPa considered here, independent passage of one pulse through another occurs.

Figure 9 shows the results of simulating the propagation of a nonlinear pulse with an initial Gaussian shape, the amplitude of $p_0 = 3.3$ MPa, and the duration of 5 μs in a medium with memory ($\eta = 1.05$, $\alpha_0 =$ 0.45 dB/cm, $c_0 = 1578$ m/s, $\rho_0 = 1060$ kg/m^3) (solid curves) and in a low-viscosity medium ($\eta = 0$, $c_0 =$ 1578 m/s, $\rho_0 = 1060$ kg/m^3) (dashed curves) and its reflection from a soft acoustic boundary. The figure illustrates the pulse profiles initially traveling in the x direction (profiles (1)–(3)) and after reflection, in the reverse direction (profiles (4)–(6)). As one can see, for $x = x_p$ during propagation in the medium with memory, the shock character of a direct wave (profile (2)) is retained; however, its shape differs from the case of propagation in a lossless medium: the pulse amplitude is lower, and the shock front forms later.

For $x = 2x_p$, the relaxation process leads to the fact that the form of profile (3) behind the shock front becomes significantly rounded. When reflecting from a soft boundary, the pulse changes its polarity, the compression phase converts to the decompression phase (profile (4)), and for $x = 3x_p$, the shock front for a wave traveling to the left (5) is smeared. Finally, for $x = 4x_p$, the pulse (6) becomes more wedge-shaped in the decompression phase, with notable steepening of its trailing edge.

Figure 10 shows an example of reflecting a shock wave pulse of several cycles from a soft boundary that mimic a cavitation cloud or a boiling vapor bubble that forms in biological tissue exposed to HIFU for its mechanical disintegration (histotripsy) [24, 25]. The pulse shape corresponds to that observed in experiment: the initial amplitude of the pulse shock front is 50 MPa, the frequency is 2 MHz, and the duration is 4 μs [24]. Each of the cycles has a characteristic shape corresponding to nonlinear-diffractive distortions of the wave profile at the focus of a high intensity ultra-

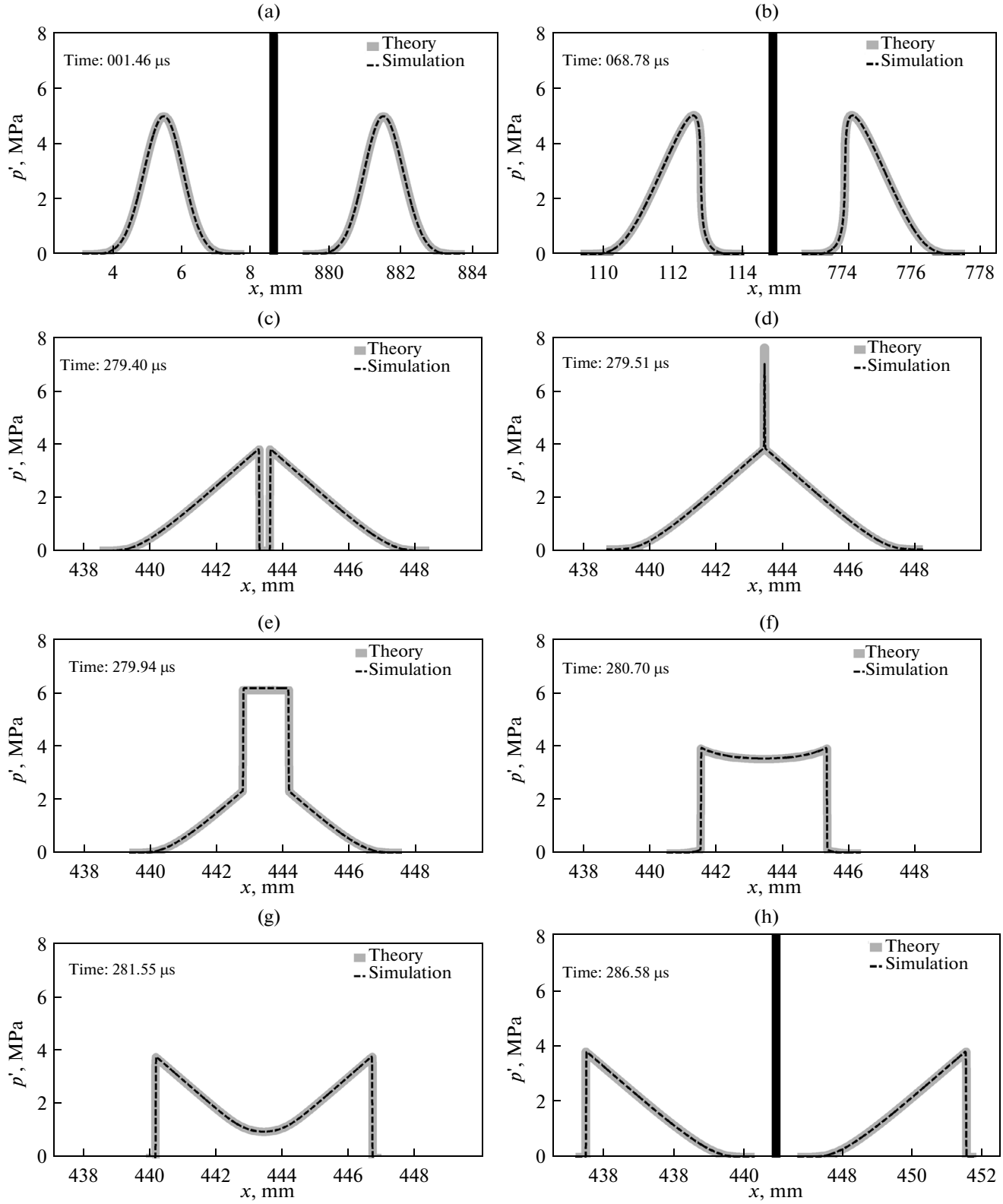

Fig. 8. Acoustic pulse waveforms for counterpropagating Riemann waves at different time instants t, that correspond to different distances $8x_p$ ($t = 1.46$ μs) (a), $6x_p$ ($t = 68.78$ μs) (b), $0x_p$ ($t = 279.4$ μs) (c); their interaction ($t = 279.51$ μs) (d), 279.94 μs (e), 280.7 μs (f), 281.55 μs (g); and pulse propagation after the interaction ($t = 286.58$ μs) (h).

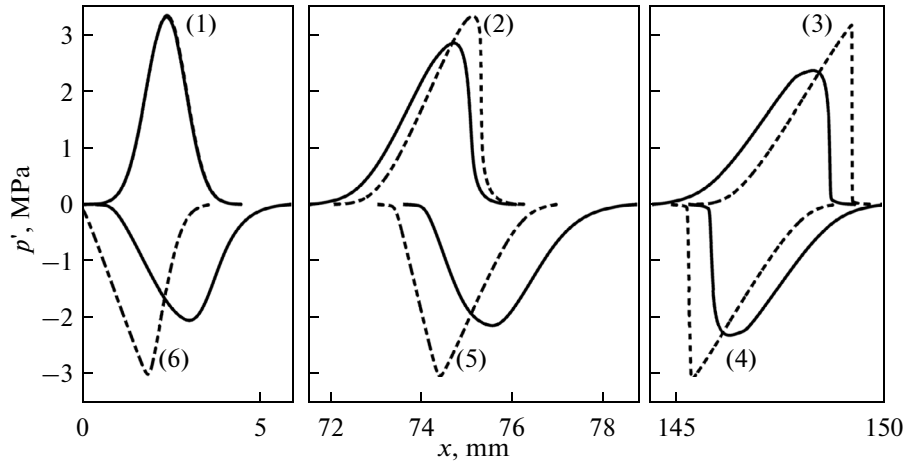

Fig. 9. Propagation of the initial Gaussian pulse with an amplitude of $p_0 = 3.3$ MPa and duration of 5 μs in a nonlinear medium with memory ($\eta = 1.05$, $\alpha_0 = 0.45$ dB/cm, $c_0 = 1578$ m/s) (solid curve) and in a lossless medium ($\eta = 0$, $c_0 = 1570$ m/s) (dashed curve) and its reflection from a soft boundary. The profiles are shown at various distances: $x = 2.5$ mm (1); $x = x_p$ (x_p is the shock formation distance) (2); $x = 2x_p$ (3); $x = 2x_p$ (reflected wave) (4); $x = 3x_p$ (5); $x = 4x_p$ (6).

sound beam: a high narrow peak positive pressure behind the shock front and a smooth rarefaction phase of substantially smaller amplitude. Two propagation media were considered: a lossless medium (black dashed curve), and an absorptive medium (solid gray curve) obeying a power law absorption with an exponent of $\eta = 1.05$ with the same parameter of acoustic nonlinearity of $\varepsilon = 1$, the sound speed of $c_0 = 1578$ m/s, and the ambient density of $\rho_0 = 1060$ kg/m^3. The figure illustrates the change in pulse polarity during reflection: superposition of the high-amplitude peak on the negative phase of the incident wave results in a sharp increase in the peak negative pressure (Fig. 10c). This effect can intensify cavitation phenomena near the boundary and can explain one of the main mechanisms of mechanical tissue damage [24,

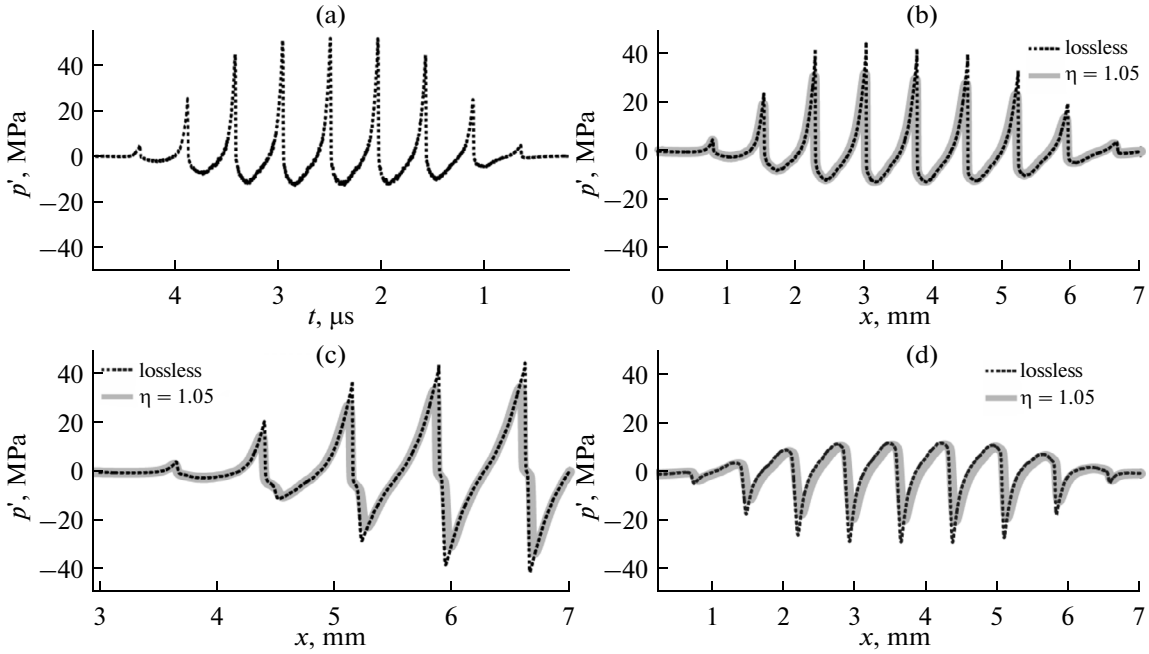

Fig. 10. Nonlinear propagation of the initial shockwave pulse $p'(x = 0, t)$ for $x = 0$ in a lossless medium $\eta = 0$ (dashed gray curve) (a) and in a lossy medium obeying a power law absorption with an exponent of $\eta = 1.05$ (solid gray curve). Pulse waveforms are shown at different time instants t corresponding to propagation in the positive direction of axis x (b); interference with a pulse reflected from a soft boundary (c), and formation of sharp peaks of negative pressure during propagation of a reflected pulse with a changed polarity in the reverse direction x (d).

25]. As mentioned above, in the case of a medium with power law absorption (solid gray curve), i.e., a medium with memory, dispersion leads to the change of the waveform behind the shock front. The wave front becomes significantly rounded in the compression phase, the position of the wave maximum is delayed comparing to the shock front in the positive half-periods (Fig. 10c), and the pulse itself is delayed from the pulse propagating in the nondispersive medium (dashed black curve). Reflection of the wave from a soft boundary leads to a change in polarity and smearing of its wave front (Figs. 10c, 10d).

4. CONCLUSIONS

A new approach that enables calculation of the memory function in the integral law of losses proceeding from the known frequency dependence of absorption and fulfilling the causality principle is presented. A system of equations for one-dimensional waves that accounts for the effects of nonlinearity, absorption, and dispersion is obtained. A finite difference algorithm for numerical simulation of the system taking into account the reflection of waves from the impedance boundary is developed. The algorithm is tested by solving a number of benchmark nonlinear acoustic problems that have analytical solutions. The test results show the good accuracy of the algorithm. Propagation of a nonlinear pulse in a medium like biological tissue and its reflection from a soft boundary is simulated as an illustration to the tissue damage mechanism during histotripsy.

Compared to known models based on nonlinear equations of the evolution type, the developed numerical model does not have any restrictions on the directionality of the sound waves. The system of equations and the algorithm can also be used to simulate wave propagation in media with spatially distributed inhomogeneities. The proposed model makes it possible to study a wider class of practically important problems of medical acoustics where it is necessary to account for reflection and scattering effects.

ACKNOWLEDGMENTS

The work was supported by the Russian Foundation for Basic Research (projects nos. 12-02-31830-mol_a and 13-02-00183) and the grants from the President of the Russian Federation (no. 14.124.13.5895-MK) and the Dynasty Foundation.

REFERENCES

1. *Physical Principles in Ultrasound Medicine,* Ed. by K. Hill, D. Bember, and G. Haar (Wiley, London, 2004), 2nd ed.
2. M. R. Beiley, V. A. Khokhlova, O. A. Sapozhnikov, S. G. Kargl, and L. A. Crum, Acoust. Phys. **49**, 369 (2003).
3. O. V. Rudenko, Phys.-Usp. **50**, 359 (2007).
4. M. A. Averkiou, in *Proc. IEEE Int. Ultrasonics Symp., 2000*, Vol. 2, pp. 1563–1572.
5. V. A. Khokhlova, A. E. Ponomarev, M. A. Averkiou, and L. A. Crum, Acoust. Phys. **52**, 481 (2006).
6. M. A. Averkiou and R. O. Cleveland, J. Acoust. Soc. Am. **106**, 102 (1999).
7. S. Ginter, M. Liebler, E. Steiger, T. Dreyer, and R. Riedlinger, J. Acoust. Soc. Am. **111**, 2049 (2002).
8. E. A. Filonenko and V. A. Khokhlova, Acoust. Phys. **47**, 468 (2001).
9. O. V. Rudenko and S. N. Gurbatov, Acoust. Phys. **58**, 242 (2012).
10. O. V. Rudenko, S. N. Gurbatov, and I. Yu. Demin, Acoust. Phys. **59**, 584 (2013).
11. I. M. Hallaj and R. O. Cleveland, J. Acoust. Soc. Am. **105**, L7 (1999).
12. L. Demi, K. W. A. van Dongen, and M. D. Verweij, J. Acoust. Soc. Am. **129**, 1221 (2011).
13. O. V. Rudenko, S. I. Soluyan, and R. V. Khokhlov, Akust. Zh. **20**, 449 (1974).
14. M. O'Donnel, E. T. Janes, and J. G. Miller, J. Acoust. Soc. Am. **63**, 1935 (1978).
15. M. D. Collins, J. Acoust. Soc. Am. **84**, 2114 (1988).
16. T. L. Szabo, J. Acoust. Soc. Am. **97**, 14 (1995).
17. H. A. Jongen, J. M. Thijssen, M. van den Aarssen, and W. A. Verhoef, J. Acoust. Soc. Am. **79**, 535 (1986).
18. R. O. Cleveland, M. F. Hamilton, and D. T. Blackstock, J. Acoust. Soc. Am. **99**, 3312 (1996).
19. G. F. Pinton, J. Dahl, S. Rosenzweig, and G. E. Trahey, IEEE UFFC **56**, 474 (2009).
20. W. Chen and S. Holm, J. Acoust. Soc. Am. **115**, 1424 (2004).
21. B. E. Treeby and B. T. Cox, J. Acoust. Soc. Am. **127**, 2741 (2010).
22. B. E. Treeby, J. Jaros, A. P. Rendell, and B. T. Cox, J. Acoust. Soc. Am. **131**, 4324 (2012).
23. I. Drumm, *Finite Difference Time Domain Tutorial* (EPSRC Summer School, 2007).
24. T. D. Khokhlova, M. S. Canney, V. A. Khokhlova, O. A. Sapozhnikov, L. A. Crum, and M. R. Bailey, J. Acoust. Soc. Am. **130**, 3498 (2011).
25. A. D. Maxwell, T.-Y. Wang, C. A. Cain, J. B. Fowlkes, O. A. Sapozhnikov, M. R. Bailey, and Z. Xu, J. Acoust. Soc. Am. **130**, 1888 (2011).

Translated by A. Carpenter